Journal of Porous Materials (2019) 26:803–811
https://doi.org/10.1007/s10934-018-0681-5

Novel route of synthesis of Sn-coated SBA-15

Marek Kosmulski[1] · **Edward Mączka**[1]

Published online: 3 October 2018

Abstract
A series of Sn-modified SBA-15, was studied. On top of Sn-only modified materials, several materials were modified with Sn and then Ti or with Sn and then Al. The new materials were obtained by adsorption of vapors of metal chlorides on SBA-15 (at 30–110 °C), and hydrolysis of adsorbed chlorides by water vapor at 25 °C, and then evaporation of left-overs of volatile compounds at 140 °C. The Sn-modified SBA-15 had lower specific surface area, and a higher thermal stability than the original silica. Even in materials containing substantial amount of Sn, the presence of crystalline phases representing Sn compounds was not detected by XRD. In contrast, rutile and anatase were observed in Sn- and Ti-modified SBA-15 while crystalline phases representing Ti compounds were not detected when Ti was deposited directly on SBA-15 (not modified with Sn). The profiles of Sn concentration across the particles of Sn-modified SBA-15 indicate that Sn is located in the pores rather than on the external surface.

Keywords Silica · Tin oxide · Rutile · Anatase · Specific surface area · ζ Potential

1 Introduction

Mesoporous silicas modified with metals have been extensively studied for many decades, and tin is among the metals, most frequently used to modify porous silicas. Introduction of MCM-41 [1], SBA-15 [2] and of other well-defined and high-specific-surface-areas (SSAs) silicas in the 1990s increased the interest in metal-modified silicas. Typically Sn-modified silicas are obtained by impregnation of the support with solution of soluble Sn compound [3] followed by drying and calcination. The interest in metal-modified porous silicas peaked in the beginning of this century, and now it is slowly declining, but Sn-modified porous silicas remain an active field, especially in view of their catalytic properties.

Very recently Li et al. [4] obtained composites with 0.4–1.6% Sn by mass by addition of $SnCl_2$ to P123–HCl solution in course of a standard SBA-15 synthesis, and their composites had slightly lower SSA and total pore volume than the SBA-15 without tin obtained by the same method. They also studied a Sn-modified specimen obtained by incipient wetness impregnation, and their materials were used as supports for Pt-catalysts for propane dehydrogenation.

Pang et al. [5] obtained composites with Si/Sn molar ratios from 130 to 394 by impregnation of SBA-15 with ethanolic solution of $SnCl_4$ pentahydrate. Their composites had slightly lower SSA and identical total pore volume as the original SBA-15. They also studied a Sn-modified specimen obtained by incipient wetness impregnation, and their materials were used as catalysts for conversion of carbohydrates to methyl lactate.

Xu et al. [6] obtained composites with Si/Sn ratios of 13 and 53 by impregnation of SBA-15 with solution of dimethyldichlorostannate and of trimethylamine in *p*-xylene followed by washing, and then by calcination in oxygen. Their composites had substantially lower SSA than the original SBA-15 in spite of low Sn fraction. Their materials were used as catalysts for hydrogenation of levulinic acid to γ-valerolactone.

Skoda et al. [7] obtained composites with 43% Sn by mass by addition of tetrakis(diethylamido)tin to Si-precursor in course of synthesis, and they studied catalytic performance of their composite material in aminolysis of styrene oxide with aniline.

✉ Marek Kosmulski
marek@kosmulski.org

Edward Mączka
e.maczka@pollub.pl

[1] Lublin University of Technology, Nadbystrzycka 38A, 20-618 Lublin, Poland

Chen et al. [8] obtained composites with Si/Sn ratios from 21 to 132 by addition of $SnCl_4$ to P123–HCl solution in course of a standard SBA-15 synthesis, and they also obtained Sn-modified MCM-41. The Sn-modified SBA-15 had slightly lower SSA and total pore volume than the SBA-15 without tin, and the Sn-modified MCM-41 had substantially lower SSA and total pore volume than the MCM-41 without tin obtained by the same method. Their materials were used as catalysts for oxidation of cyclohexanone to ε-caprolactone.

Srinivasan et al. [9] obtained composites with 5–17% Sn by impregnation of five different lots of SBA-15 with dilute aqueous $SnCl_4$ solution followed by reduction with solution of sodium borohydride. The product was filtered out, washed with water, and oxidized at 100 °C in air. Their materials were used as catalysts for photochemical degradation of rhodamine B.

In view of their extraordinary catalytic properties, Sn–porous silica composites deserve special attention. In this study we present a novel method of preparation of such composites, which is based on our previous experiments with other metals [10, 11]. Namely in contrast with other studies which used one-pot synthesis (Sn precursor added in course of synthesis of porous silica) or post-synthesis impregnation of porous silica with solution of Sn precursor, we deposited volatile metals or volatile metal compounds on pre-synthesized silica. Our method can be used to deposit practically every metal, but so far we only presented composites containing Cd, Zn, Ti and Al. In this study we focus on Sn-modified SBA-15. With its boiling point at 114 °C, and vapor pressure of 24 hPa at 20 °C, tin(IV) chloride is a convenient precursor of tin, which can be deposited on silica from gas phase even at room temperature.

2 Methods

2.1 Deposition of Sn, Al and Ti on SBA-15

We used the same lot of SBA-15 (produced using a standard recipe) as in our previous work [11]. Silica was stored for 6–9 months in a plastic bottle before deposition of Sn. The method of deposition of metals onto silica by adsorption of vapors of their chlorides and then their hydrolysis is similar to that described in older literature [12]. A portion of 90–250 mg of SBA-15, was transferred into a 15-mL glass beaker, and 90–210 mg of anhydrous metal chloride was transferred into another 15-mL beaker. The beakers were closed in an air-tight 300 mL glass flask. These operations were performed as quickly as possible to avoid reaction between anhydrous chlorides and atmospheric moisture. The closed conical flask with both beakers was thermostated in a laboratory drying oven at certain temperature, and for certain time, and then cooled down to room temperature. Two different geometries produced different composites at otherwise identical conditions. In geometry 1 (most experiments) the 15 mL beakers were broad and short, and in geometry 2 (a few experiments) they were narrow and tall. The SBA-15 with metal chloride adsorbed on it, was allowed to react with vapor of 2 M KOH for 1 day in a desiccator, and it was dried for 1 day at 140 °C. A few materials were dried at lower temperatures after hydrolysis, but the low drying temperature was proved insufficient for complete removal of volatile compounds in Sn-rich composites (see Results section for more detail). The amount of metal oxide deposited on silica was determined on mass basis. Several Sn-SBA-15 composites were further processed as described above, but with $TiCl_4$ (deposition at 30–50 °C) or with $AlCl_3$ (deposition at 110 °C) as metal precursors. A few composites were heated at 600–1000 °C to test their thermal stability.

2.2 Characterization of Sn-modified SBA-15

XRD patterns of the composites were collected with Empyrean from PANalytical. The BET SSA and pore volume were measured with Gemini V (Micromeritics). A few composites were dispersed in 10^{-3} M NaCl to measure the ζ potential and particle size as a function of pH by means of Malvern Zetasizer (Malvern, UK). Tecnai G^2 20 from FEI (Hillsboro, Oregon) was used to obtain microscopic images of the original and Sn-modified SBA-15 containing 38.75% of SnO_2 by mass ($SiO_2 = 100\%$). This material was obtained by adsorption of tin chloride at 50 °C for 1 h, and it has a SSA of 650.5 $m^2\ g^{-1}$. The ethanolic dispersion of pulverized material was ultrasonified, and deposited on Lacey C/F polymer-coated Cu grid. The images in bright field mode with CCD detector, and in STEM mode with HAADF detector were recorded. Concentration profiles of O, Si, and Sn across a particle of the same Sn-modified SBA-15 were studied using TEM–EDS (energy dispersive X-ray spectroscopy) method.

3 Results and discussion

3.1 Original and calcined SBA-15

The calcination of SBA-15 at temperatures below 700 °C had rather insignificant effect on its properties, while modification at temperatures above 700 °C resulted in decrease in the SSA and in the pore volume. The detailed results are presented elsewhere [11], and they are in line with numerous results reported in the literature.

3.2 Preparation of Sn-modified SBA-15

The specimens of Sn-modified SBA-15 after hydrolysis of adsorbed $SnCl_4$ were dried at various temperatures in order to establish the conditions necessary to completely remove the volatile compounds from silica. The specimens underwent 1 h drying cycles at 80, then 90, then 100, then 110, and then 120 °C, followed by 20 h at 130 °C and 24 h at 140 °C. The decrease in mass of two specimens of Sn-modified SBA-15 (17 and 15% SnO_2 by mass, respectively) on drying is illustrated in Fig. 1. These results show that even after 20-h drying at 130 °C the process of removal of volatile compounds was not 100%-complete. Therefore all specimens were dried for at least 1 day at 140 °C in order to completely remove volatile compounds. Figure 1 illustrates the behavior of the components with high Sn concentration. In specimens with low (e.g., 3%) SnO_2 concentration already drying at 90 °C for 1 h led to complete removal of volatile compounds, that is, further heating at 100, 110 °C, etc. had rather insignificant effect on the mass of the composite. Also in Ti- and Al-modified SBA-15 (discussed in detail in our previous study [11]), drying at 90 °C for 1 h was sufficient to completely remove volatile compounds.

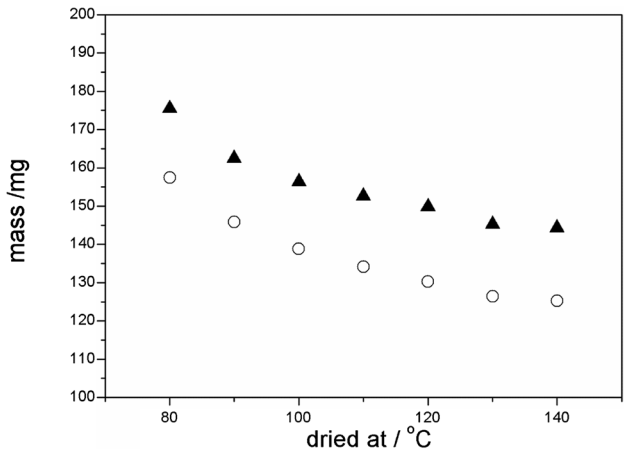

Fig. 1 Mass of two specimens of Sn-modified SBA-15 (white circles 17% SnO_2, black triangles 15% SnO_2) dried at various temperatures after hydrolysis of $SnCl_4$

3.3 Sn-modified SBA-15

The properties of Sn-modified SBA-15, obtained by deposition of 0.1 mL of $SnCl_4$ for 30 min at 30–50 °C in different geometries (see experimental) on (about) 100 mg of SBA-15 are summarized in Tables 1 and 2. The specimens presented in Table 2 are different than those presented in Table 1, and they were further modified with Ti or with Al.

Preparation at the same conditions (amount of $SnCl_4$, time and temperature of deposition, geometry) produced materials with similar fraction of SnO_2 (with substantial scatter).

The presence of Sn in SBA-15 resulted in linear decrease in the SSA of silica (correlation coefficient of 0.92) with the mass fraction of SnO_2. The micropore volume was rather insensitive to the presence of Sn, and it showed random scatter rather than systematic trend when plotted against the amount of SnO_2. The correlation between SSA and the amount of SnO_2 in the composite is presented in Fig. 2.

The XRD patterns of Sn-modified SBA-15 are shown in Figs. 3 and 4. The small angle XRD patterns (Fig. 3) indicate the hexagonal structure in Sn-SBA-15, and the presence of Sn had rather insignificant effect on the *d*-spacing. The wide-angle XRD patterns of Sn-modified SBA-15 (Fig. 4) did not reveal any peaks representing Sn-compounds in spite of substantial mass fraction of Sn in the composite materials. Apparently Sn occurs in the composite as a thin uniform layer on the surface of silica rather than as large crystalline aggregates. There is a shoulder in the XRD pattern of the specimen containing 26% of SnO_2, at 2 θ of about 10° which does not occur in other patterns, but this feature does not prove the presence of crystalline Sn compound(s).

Table 1 Properties of Sn-modified SBA-15

Adsorption of $SnCl_4$			% SnO_2 (SiO_2 = 100%)	SSA ($m^2\ g^{-1}$)	Pore volume ($cm^3\ g^{-1}$)	Micropore volume ($cm^3\ g^{-1}$)	Average pore diameter (nm)
t (°C)	Time (h)	geometry					
None			None	910.1	1.035	0.104	4.55
30	0.5	1	26.4	694.7	0.83	0.078	4.78
30	0.5	1	10.4	791.5	0.933	0.095	4.72
30	0.5	1	11.7	777.5	0.929	0.091	4.78
30	0.5	1	16.1	761.6	0.923	0.092	4.85
30	0.5	2	4.1	881.7	1.015	0.11	4.61
30	0.5	2	5.3	846.9	0.991	0.107	4.68
35	0.5[a]	1	10.9	733.4	0.915	0.082	4.99

[a]226 mg of SBA-15

Table 2 Properties of Ti-modified Sn-SBA-15 and of Al-modified Sn-SBA-15

First deposition		Second deposition		SSA ($m^2\ g^{-1}$)	Pore volume ($cm^3\ g^{-1}$)	Micropore volume ($cm^3\ g^{-1}$)	Average pore diameter (nm)
Metal	% of metal oxide ($SiO_2 = 100\%$)	Metal	% of metal oxide ($SiO_2 = 100\%$)				
None	None	None	None	910.1	1.035	0.104	4.55
Sn	10.4	None	None	791.5	0.933	0.095	4.72
Sn	10.4	Ti	27.6	595.2	0.613	0.085	4.12
Sn	11.7	None	None	777.5	0.929	0.091	4.78
Sn	11.7	Ti	17.7	611.7	0.678	0.081	4.43
Sn	16.1	None	None	761.6	0.923	0.092	4.85
Sn	16.1	Ti	8.3	746	0.977	0.082	5.24
Sn	14.9	None	None	667	0.813	0.07	4.88
Sn	14.9	Ti	25.9	549.3	0.636	0.059	4.63
Sn	17.2	None	None	706.3	0.853	0.073	4.83
Sn	17.2	Ti	37.2	546	0.624	0.064	4.57
Sn	2.9	None	None	833.7	0.956	0.104	4.59
Sn	2.9	Ti	3	833.2	0.975	0.104	4.68
Sn	19.9	None	None	710	0.891	0.064	5.02
Sn	19.9	Al	11.7	708.3	0.907	0.07	5.12
Sn	15.2	None	None	716.9	0.873	0.075	4.87
Sn	15.2	Al	14	718.2	0.933	0.079	5.19
Sn	20.7	None	None	641.9	0.813	0.061	5.06
Sn	20.7	Al	4.7	670.2	0.82	0.068	4.89

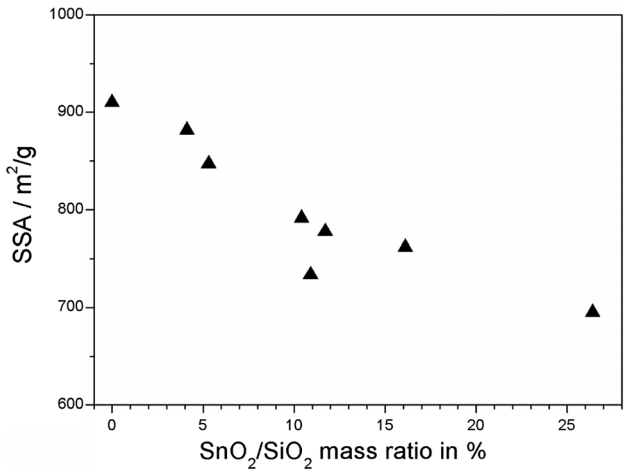

Fig. 2 Correlation between the amount of deposited SnO_2 and the specific surface area of Sn-modified SBA-15

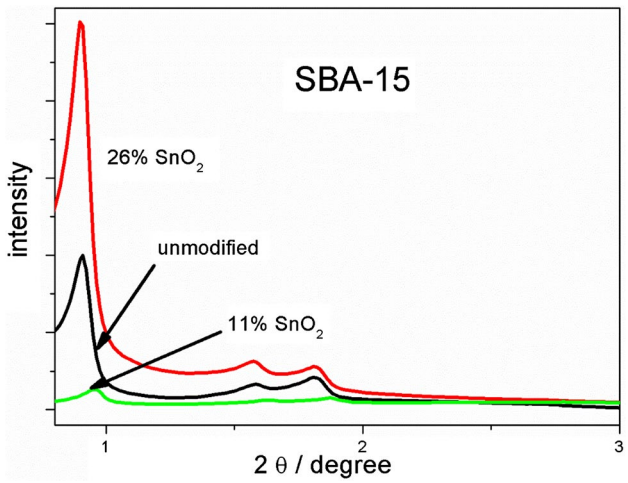

Fig. 3 Small-angle XRD patterns of original and of Sn-modified SBA-15

3.4 Thermal stability

Figure 5 shows the result of calcination at different temperatures on the SSA of a Sn-modified material containing 11% of SnO_2. The calcination at temperatures up to 800 °C had rather insignificant effect on the SSA while calcination at higher temperatures depressed the SSA. Apparently Sn-modified SBA-15 is more resistant to calcination than the original SBA-15 (Sect. 3.1), but temperatures above 800 °C cause degradation of both modified and unmodified silica.

3.5 Sn- and Ti-modified SBA-15 and Sn- and Al-modified SBA-15

Several materials were obtained using $AlCl_3$ to deposit alumina, and $TiCl_4$ to deposit titania on Sn-SBA-15 (obtained

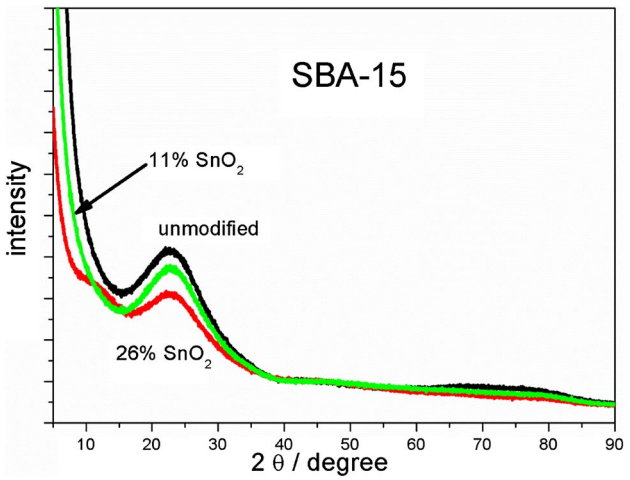

Fig. 4 Wide-angle XRD patterns of original and of Sn-modified SBA-15

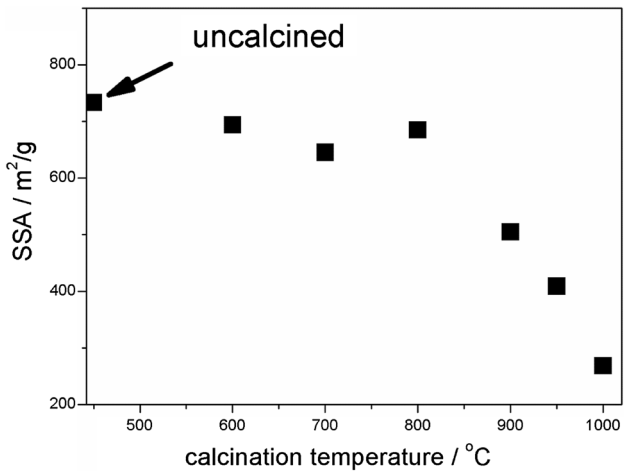

Fig. 5 The effect of calcination temperature on the SSA of a Sn-modified SBA-15 containing 11% of SnO_2

according to the procedure described in the experimental part). Materials with Sn deposited on Al-SBA-15 or on Ti-SBA-15 were not studied. The method of deposition of Ti and Al was similar to the method used for deposition of Sn, and it was described in more detail in our previous paper [11]. The properties of the original SBA-15, of Sn-SBA-15 which were used as supports, and of the final products (Sn- and Ti-modified SBA-15 and Sn- and Al-modified SBA-15) are summarized in Table 2. The Sn-SBA-15 presented in Table 2 are different specimens from those presented in Table 1. Most Sn-SBA-15 were obtained by deposition of $SnCl_4$ at 30 or 35 °C, and in the specimen with 15.2% SnO_2 the deposition was at 40 °C, and in the specimens with 19.9 and 20.7% SnO_2 the deposition was at 50 °C. The properties of supports (Sn-only-SBA-15) are followed by the properties of the final products (Sn- and Ti-SBA-15 and Sn- and Al-SBA-15) obtained from these supports.

$TiCl_4$ and $AlCl_3$ are adsorbed onto Sn-modified silicas to similar degree as onto the original SBA-15, that is, the mass% of titania or of alumina in materials obtained from Sn-modified silicas is similar as in materials obtained from the original SBA-15 at the same conditions (amount of metal chloride, time and temperature of deposition).

The modification of SBA-15 with metals resulted in nearly linear decrease in the SSA of silica (correlation coefficient of 0.89) with the total amount of metal oxides, and the micropore volume decreased on Ti-modification. The correlation between SSA and the amount of metal oxides is illustrated in Fig. 6. The slope of the trend line (about 10 $m^2\ g^{-1}$ per 1% of metal oxide) in Fig. 6 is similar to that observed in Fig. 2. As we discussed in our previous papers, the decrease in the SSA ($m^2\ g^{-1}$) is in line with the specific density of tin (7 g cm^{-3}) and of titanium and aluminum (4 g cm^{-3}) oxides, which is substantially higher than that of silica.

The small angle XRD pattern of SBA-15 was rather insensitive to the Sn- and Ti-modification as illustrated in Fig. 7. It indicates the hexagonal structure in Sn- and Ti-SBA-15, and the presence of Sn and Ti had rather insignificant effect on the *d*-spacing. The wide-angle XRD pattern of Sn- and Ti-modified SBA-15 (Fig. 8) did not reveal any peaks representing Sn-compounds, and this result suggests that tin is present in the composite as a thin, uniform layer on the surface of silica. This result is in line with the results observed with Sn-only modified SBA-15 (Fig. 4).

Crystallization of titanium dioxide was observed on Sn-modified SBA-15. This result is different from the results reported in [11], in which no peaks corresponding to Ti-compounds were observed in materials obtained by the same

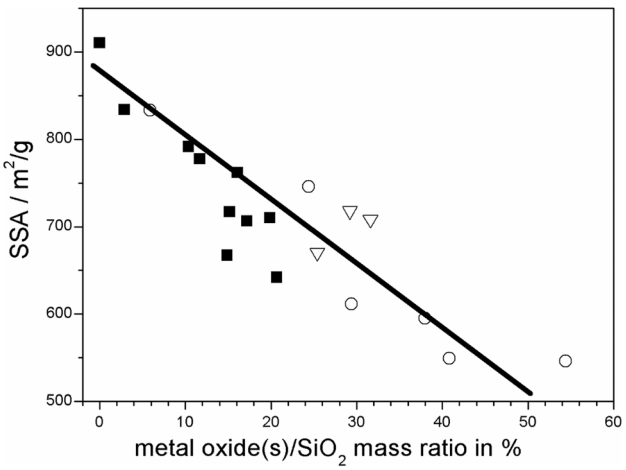

Fig. 6 Correlation between the total amount of metal oxide(s) and the specific surface area of Sn-modified SBA-15 (black squares) of Sn- and Ti-modified SBA-15 (white circles), and of Sn- and Al-modified SBA-15 (white triangles)

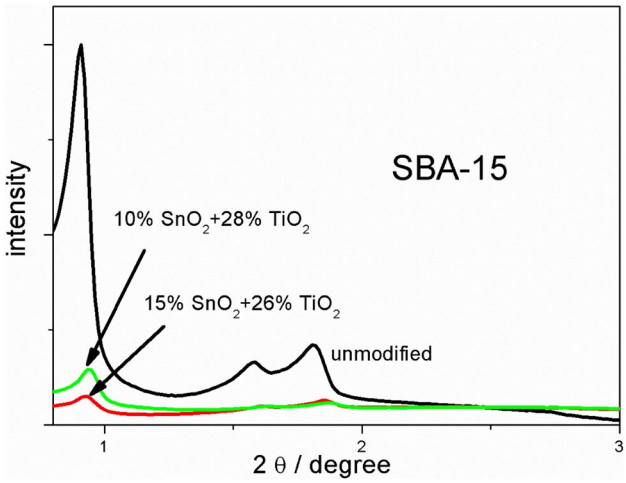

Fig. 7 Small-angle XRD patterns of Sn- and Ti-modified SBA-15 as compared with the original silica

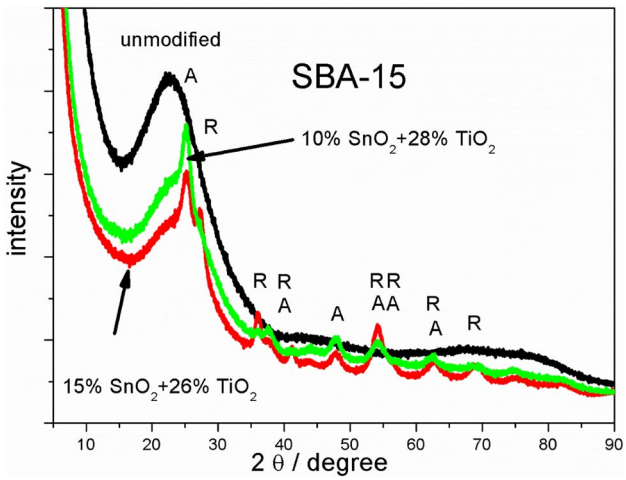

Fig. 8 Wide-angle XRD patterns of Sn- and Ti-modified SBA-15 as compared with the original silica. *A* anatase, *R* rutile

method as used in the present study, when Ti was deposited directly on SBA-15 or on Al-modified SBA-15. The peaks corresponding to Ti-compounds were not observed in Ti-modified SBA-15 even after calcination at 700 °C. Apparently the presence of Sn on the surface of SBA-15 promoted crystallization of titania in Sn- and Ti-modified materials. Cassiterite (SnO_2) is isostructural with rutile, and this may explain the difference in crystallization of TiO_2 on Sn-SBA-15 on the one hand and on bare SBA-15 on the other. Almost pure anatase with a small admixture of rutile was observed in the specimen containing 10% of SnO_2 and 28% of TiO_2, while a 42:58 anatase–rutile mixture was observed in the specimen containing 15% of SnO_2 and 26% of TiO_2. We also attempted to determine the sizes of crystallites from FWHM of the peaks shown in Fig. 8. The apparent sizes of crystallites determined from the 25° peak (anatase) and 27.5° peak (rutile) were 8 nm in the specimen containing 10% of SnO_2 and 28% of TiO_2 and 9 nm in the specimen containing 15% of SnO_2 and 26% of TiO_2. This should be emphasized that most peaks observed in anatase–rutile mixtures are results of overlap of two or more lines (from both rutile and anatase) and they are of limited significance in crystallite size determination. The crystallization of titania in Ti-modified SBA-15 was discussed in many previous studies. However, in most studies the Ti-modified SBA-15 was calcined before the XRD study, and the structure of uncalcined materials was not reported. For example Landau et al. [13] observed anatase in Ti-modified SBA-15 obtained by impregnation of porous silica with Ti-butoxide, followed by chemical solution decomposition or by internal hydrolysis, and by calcination at 500 °C. Acosta-Silva et al. [14] observed anatase in Ti-modified SBA-15 obtained by impregnation of porous silica with propanolic solution of Ti-isopropoxide, followed by addition of water at room temperature, and by calcination at 550 °C. Anatase was only observed in Ti-rich specimens (26% of titania or more). In contrast with most previous studies, our specimens were not calcined, and they were only dried at 140 °C.

The deposition of Al on Sn-SBA-15 resulted in rather insignificant change in the SSA, and in one specimen the SSA even increased on Al-deposition.

3.6 TEM images and concentration profiles

The bright-field TEM image of Sn-modified SBA-15 containing 39% of SnO_2 ($SiO_2 = 100\%$) by mass (Fig. 9) confirms the typical structure reported in the literature for unmodified and metal-modified SBA-15 materials. The feature in the upper right part shows a hexagonal network of channels, and the feature in the bottom part shows a series of parallel channels with a channel width of 9 nm similar to the *d*-spacing obtained from the position of the (100) peaks in the small-angle XRD patterns. The same channel width is seen in a dark-field STEM image of the same specimen of Sn-SBA-15 shown in Fig. 10.

The profile of Sn-modified SBA-15 in which the elementary composition across a particle was studied is illustrated in Fig. 11. This profile consists of 20 parallel channels.

The concentration of Sn along the profile shown in Fig. 11 is presented in Fig. 12, which confirms that Sn is distributed over the entire volume of a Sn-SBA-15 particle, although the distribution is not entirely uniform. The oscillatory character of the concentration of Sn reflects the presence of pores in the specimen. The elementary composition obtained by TEM–EDS method corresponds to 33% of SnO_2 ($SiO_2 = 100\%$) by mass, which is lower than 39% obtained from the gain of mass of sample on Sn deposition.

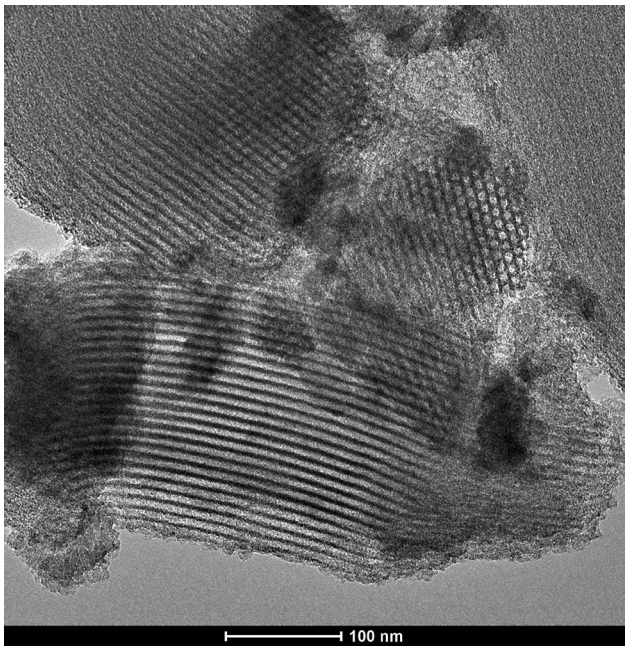

Fig. 9 Bright-field TEM image of Sn-modified SBA-15 containing 39% of SnO_2 ($SiO_2 = 100\%$) by mass

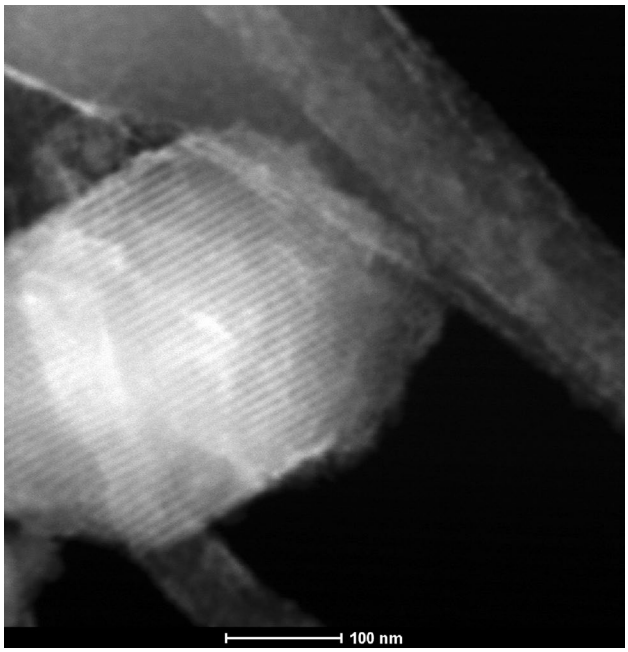

Fig. 10 Dark-field STEM image of Sn-modified SBA-15 containing 39% of SnO_2 ($SiO_2 = 100\%$) by mass

3.7 ζ Potential

The original SBA-15 and three specimens of modified SBA-15 described in the previous sections (Sn, Sn + Ti, and Sn + Al-modified) were dispersed in 10^{-3} M NaCl,

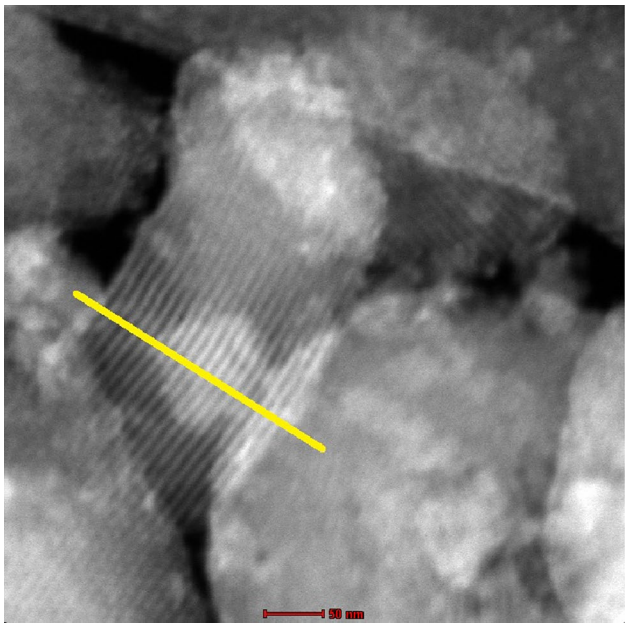

Fig. 11 Profile of Sn-modified SBA-15 containing 39% of SnO_2 ($SiO_2 = 100\%$) by mass, in which the elementary composition across a particle was studied

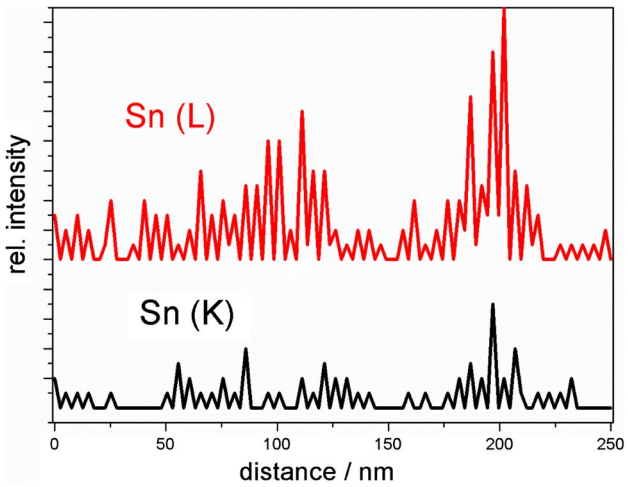

Fig. 12 The Sn concentration in a Sn-modified SBA-15 along the profile shown in Fig. 11 determined from intensity of K- and L-lines

adjusted to different pH with dilute HCl or NaOH, and the electrokinetic potential of the particles was measured. The electrokinetic curves in Fig. 13 show an IEP at pH between 3 and 4. We interpret the differences in the apparent IEP of particular specimens as a scatter of experimental points rather than as a real effect. The IEP in this range has been reported in the literature for different specimens of SBA-15 and for other silicas [15, 16]. Apparently the metal oxides in metal-modified silicas are in the pores of SBA-15 rather than on the external surface or as separate particles. This is

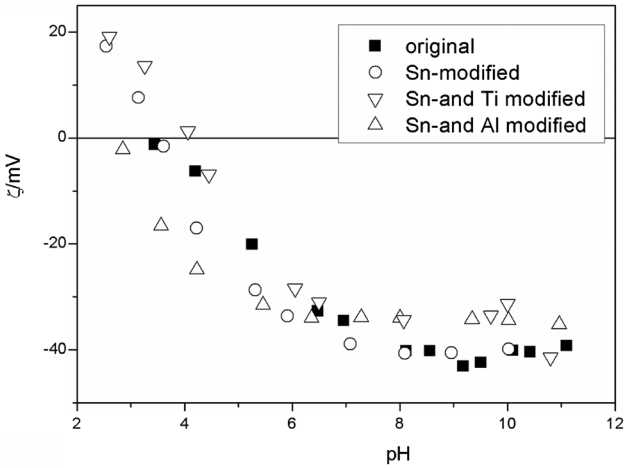

Fig. 13 ζ potential of original and of metal-modified SBA-15 dispersed in 10^{-3} M NaCl at 25 °C

well-known that deposition of metal oxide on the external surface of silica leads to higher (less negative) ζ potential, and this results in a shift in the IEP to higher pH value. Such shifts were observed for fractions of metal oxide as low as a few per cent and even a fraction of 1% by mass. This effect is more substantial for alumina (IEP at pH 9), but it is also significant for titania (IEP at pH 6) while tin oxide has an IEP at pH 4.5, that is, only slightly higher than SBA-15. The apparent IEP of Sn- and Al-modified SBA-15 shown in Fig. 13 is lower than the IEP of original silica while a shift in the IEP to high pH is expected in alumina-coated silicas (with respect to the original silica). The particle radius in dispersion was about 700 nm for all specimens shown in Fig. 13, and it was rather insensitive to pH.

4 Summary and further research

Tin is deposited on SBA-15 by evaporation and condensation of vapor of $SnCl_4$ at temperatures of 30–50 °C in a closed reactor and then by hydrolysis at room temperature. Deposition of tin depresses the SSA and total pore volume of the original silica while the effect of Sn on the volume of micropores is rather insignificant. The Sn-modified materials did not show presence of crystalline phases of Sn-compounds. The properties of Sn-modified silicas can be adjusted to specific application by varying the time and temperature of deposition and the geometry of the reactor. Sn-modified SBA-15 can also be used as a support for deposition of Ti and Al oxides on top of the SnO_2-layer. Anatase or mixture or anatase and rutile were observed in specimens obtained by condensation of $TiCl_4$ vapor on Sn-modified SBA-15 followed by hydrolysis. Crystallization of titania on Sn-modified silica at low temperatures was rather unexpected, and this phenomenon needs further research. Similar materials can be obtained from porous silicas other than SBA-15 including cheap commercial products.

Compliance with ethical standards

Conflict of interest The authors declare that they have no conflict of interest.

References

1. C.T. Kresge, M.E. Leonowicz, W.J. Roth, J.C. Vartuli, J.S. Beck, Ordered mesoporous molecular-sieves synthesized by a liquid-crystal template mechanism. Nature **359**, 710–712 (1992)
2. D.Y. Zhao, J.L. Feng, Q.S. Huo, N. Melosh, G.H. Fredrickson, B.F. Chmelka, G.D. Stucky, Triblock copolymer syntheses of mesoporous silica with periodic 50 to 300 Angstrom pores. Science **279**, 548–552 (1998)
3. M. Kumar, C. Santhosh, A. Holmen, et al., Dehydrogenation of propane over Pt-SBA-15 and Pt–Sn-SBA-15: effect of Sn on the dispersion of Pt and catalytic behavior. Catal. Today **142**, 17–23 (2009)
4. B. Li, Z. Xu, W. Chu, F. Jing, Ordered mesoporous Sn-SBA-15 as support for Pt catalyst with enhanced performance in propane dehydrogenation. Chin. J. Catal. **38**, 726–735 (2017)
5. J. Pang, M. Zheng, X. Li, L. Song, R. Sun, J. Sebastian, A. Wang, J. Wang, X. Wang, T. Zhang, Catalytic conversion of carbohydrates to methyl lactate using isolated tin sites in SBA-15. ChemistrySelect **2**, 309–314 (2017)
6. S. Xu, D. Yu, T. Ye, P. Tian, Catalytic transfer hydrogenation of levulinic acid to gamma-valerolactone over a bifunctional tin catalyst. RSC Adv. **6**, 1026–1031 (2017)
7. D. Skoda, A. Styskalik, Z. Moravec, P. Bezdicka, J. Bursik, P.H. Mutin, J. Pinkaqs, Mesoporous SnO_2–SiO_2 and Sn–silica–carbon nanocomposites by novel non-hydrolytic templated sol–gel synthesis. RSC Adv. **6**, 68739–68747 (2016)
8. T. Chen, B. Wang, Y. Li, L. Liu, S. Qiu, Hydrothermal synthesis of tin containing mesoporous silicas and their catalytic performance over Baeyer–Villiger oxidation of cyclohexanone to ε-caprolactone: comparison of Sn/MCM-41 and Sn/SBA-15. J. Porous Mater. **22**, 949–957 (2015)
9. N.R. Srinivasan, P. Majumdar, N.K.R. Eswar, R. Bandyopadhyaya, Photocatalysis by morphologically tailored mesoporous silica (SBA-15) embedded with SnO_2 nanoparticles: experiments and model. Appl. Catal. A. **498**, 107–116 (2015)
10. M. Kosmulski, E. Mączka, Uptake of vapors of Cd at 480–600 °C and of Zn at 750–880 °C by SBA-15. Microporous Mesoporous Mater. **246**, 114–119 (2017)
11. M. Kosmulski, E. Mączka, Modification of SBA-15 with vapors of aluminum and titanium chlorides. Colloids Surf. A **535**, 61–68 (2017)
12. V. Gunko, V. Zarko, V. Turov, R. Leboda, E. Chibowski, L. Holysz, E. Pakhlov, E. Voronin, V. Dudnik, Y. Gornikov,

CVD-titania on fumed silica substrate. J. Colloid Interface Sci. **198**, 141–156 (1998)
13. M.V. Landau, L. Vradman, X. Wang, L. Titelman, High loading TiO_2 and ZrO_2 nanocrystals ensembles inside the mesopores of SBA-15: preparation, texture and stability. Microporous Mesoporous Mater. **78**, 117–129 (2005)
14. Y.J. Acosta-Silva, R. Nava, V. Hernandez-Morales, S.A. Macias-Sanchez, M.L. Gomez-Herrera, B. Pawelec, Methylene blue photodegradation over titania-decorated SBA-15. Appl. Catal. B **110**, 108–117 (2011)
15. M. Kosmulski, Isoelectric points and points of zero charge of metal (hydr)oxides: 50 years after Parks' review. Adv. Colloid Interface Sci. **238**, 1–61 (2016)
16. M. Kosmulski, The pH dependent surface charging and points of zero charge. VII. Update. Adv. Colloid Interface Sci. **251**, 115–138 (2018)